Archives of Materials Science and Engineering

Volume 49
Issue 1
May 2011
Pages 15-24

International Scientific Journal
published monthly by the
World Academy of Materials
and Manufacturing Engineering

Microstructure evaluation of long-term aged binary Ag-Cu alloy

K. Labisz*, Z. Rdzawski, M. Pawlyta

Division of Materials Processing Technology, Management and Computer Techniques in Materials Science, Institute of Engineering Materials and Biomaterials, Silesian University of Technology, ul. Konarskiego 18a, 44-100 Gliwice, Poland

* Corresponding author: E-mail address: krzysztof.labisz@polsl.pl

Received 10.02.2011; published in revised form 01.05.2011

ABSTRACT

Purpose: In this work there are presented microstructure investigation results of the long aged Ag-Cu alloy used for monetary production. The purpose of this work was to determine the microstructural phase changes after 30 year ageing time, with appliance of transmission electron microscopy. Mainly the possibility of spinodal decomposition process occurrence was investigated.

Design/methodology/approach: The investigations were performed using optical microscopy for the microstructure determination. By mind of the transmission and scanning electron microscopy the phase determination was possible to achieve. Morphology investigation of the Ag-Cu matrix and phase identification using electron diffraction, EBSD technique and SEM phase contrast methods was applied.

Findings: After the long time ageing time and plastic deformation of the material there are morphological different areas of the Ag_{α} and Cu_{β} phase detected.

Research limitations/implications: The investigated material samples were examined metallographically using light microscope, SEM, TEM with different image techniques. The hardness was measured using the Rockwell hardness tester, also EDS microanalysis and electron diffraction was performed.

Practical implications: As an implication for practice use there is the possibility of application of long term ageing for mechanical properties improvement by natural ageing method. Also the comparison of microstructure change and deformation after long term ageing can deliver a new scientific view on the processes occurred in the microstructure over a long time period - spinodal decomposition can act as an example of this. Some other investigations should be performed in the future, but the knowledge found in this research shows an interesting investigation direction, where a low cost but long term treatment operations can be applied.

Originality/value: The combination of TEM investigation for silver containing alloys makes the investigation very attractive for electronic, chemical and monetary industry branches.

Keywords: Heat treatment; Surface treatment; Plastic forming; Natural ageing; Silver-copper alloy

Reference to this paper should be given in the following way:

K. Labisz, Z. Rdzawski, M. Pawlyta, Microstructure evaluation of long-term aged binary Ag-Cu alloy, Archives of Materials Science and Engineering 49/1 (2011) 15-24.

MATERIALS

1. Introduction

One of the most important strengthening mechanisms present in silver-copper alloys is spinodal decomposition. It is a phase transformation in which both phases have equivalent symmetry but differ only in composition. This transformation has been theoretically described by Cahn and Hilliard. Binder at all. generalised the linearised Cahn-Hilliard theory to the case of the existence of a slowly relaxing variable. Their calculations, presented graphically in 2D simulation in Fig. 1 show that the instability of the system is not of the standard diffusive type, but rather it is controlled by the relaxation of the slow structural variable. Recently, Cahn-Hillard theory has been modified by taking into account the relaxation of diffusion flux to its local steady state. The flux is considered as an independent thermodynamic variable in consistency with the extended irreversible thermodynamics. As a result, a partial differential equation of a hyperbolic type for phase separation with diffusion has been derived that can be called "a hyperbolic model for spinodal decomposition". Theoretically, this model can predict spinodal decomposition for short periods of time, large characteristic velocities of the process, large concentration gradients, or deep supercoolings at the earliest stages of decomposition. A comparative analysis for both Cahn-Hilliard's parabolic model and the hyperbolic model (modified Cahn-Hilliard) of spinodal decomposition. As a test for the hyperbolic model (Fig. 2), its predictions are compared with experimental data in this paper, where for example the distance between the ordered precipitations should be equal ~ 15 nm [1-8].

A pair of partially miscible liquids, i.e. liquids that do not mix in all proportions at all temperatures, shows in a temperature-composition diagram a miscibility gap where phase separation occurs (Figs. 3 and 4). Gibbs showed that the condition for stability (or metastability) in respect to continuous change of phase is that the second derivative of the free energy of mixing to be positive. If negative, the system is unstable. If zero, the spinodal is defined [9-12].

Diffusion processes, like spinodal decomposition and Ostwald ripening are in contrast to IMC-formation (intermetallic-formation) phase separation and coarsening exclusively driven by aspects of thermodynamical stability and interfacial energy minimisation. The resulting “composite” of different phases can be interpreted as a “particle reinforced material” in which the stiffer phase acts as the reinforcement. Unfortunately mechanical failure, such as cracks, favourably grow along the phase boundary which result, among other reasons, from thermal mismatching. Thus the benefit of phase dispersion is limited by a critical phase size [13-18].

As shown in Fig. 3 from a thermodynamical point-of-view a binary alloy A-B decomposes below a critical temperature T_{crit} into two equilibrium phases α and β due to a miscibility gap resulting in a gain of the Gibbs free energy G(y, T), which is a function of particle concentration y ≡ yB (with yA+yB = 1) and temperature T.

Without loss of generality we consider an initially eutectic mixture (Tcrit ≡ Teut), which is quenched from T > Teut (liquid) to T < Teut (solid). In the liquid state the Gibbs free energy of the system is given by the energetically advantageous convex curve illustrated in Figure 3a. Obviously the mixture is stable to all fluctuations. This fact becomes evident if we imagine in Figure 3a a fluctuated two-phase-system, represented by the concentrations y=1 and y2 in the neighbourhood of the original one-phase-state given by y0. The resulting energy G of the two-phase-mixture is given by the energetically disadvantageous connecting line. Therefore the system remains in the one-phase-state with the concentration y=0. This fact changes for the solid state as illustrated in Figure 3c. In this case the crucial curve of G(y, T) is piecewise concave. This region is called the spinodal area, enclosed by the spinodal concentrations y_{sp}.

a)

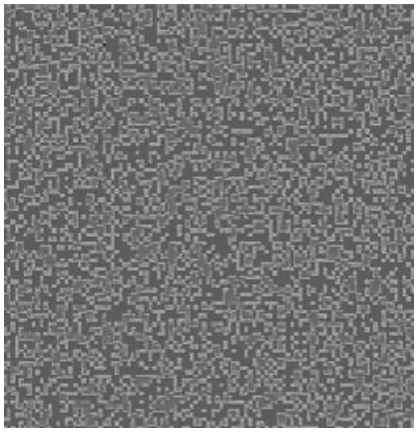

b)

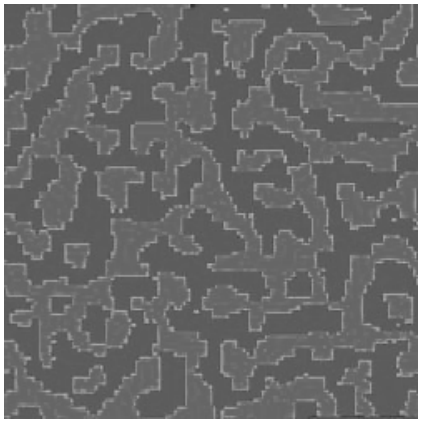

Fig. 1. Two-dimensional simulation snapshots of spinodal decomposition calculated by D. Landy and L. Wang a) state before and b) after for the decomposition process [3]

Figure 3c illustrates the construction of the equilibrium concentrations yα/β of the two solid phases α and β. The process, during which a one-phase system is quenched into the unstable area and subsequently decomposes into different equilibrium phases is called spinodal decomposition.

Figure 3b displays the intermediate situation for the critical temperature T = Teut, which is passed during the quenching process. Here the common tangent rule yields three equilibrium concentrations, so that three phases coexist within the systems: two solid phases with the concentrations yα/β and one liquid phase with the concentration y=0 [2, 19-21].

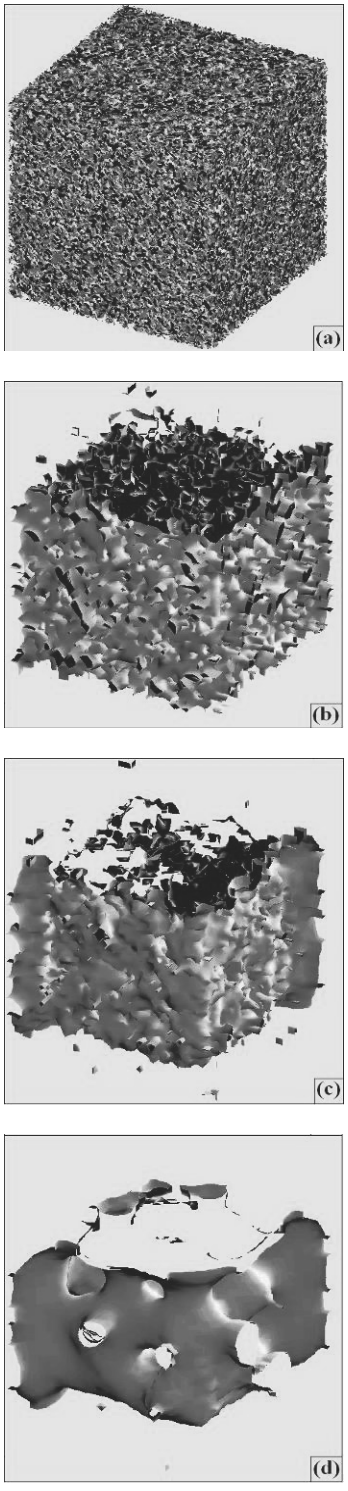

Fig. 2. Three-dimensional evolution of spinodally decomposed liquid. The modelling is provided using a "hyperbolic" model for phase separation. Snapshots for the decomposed (blue) phase are shown for various computational times [3, 4]

a)

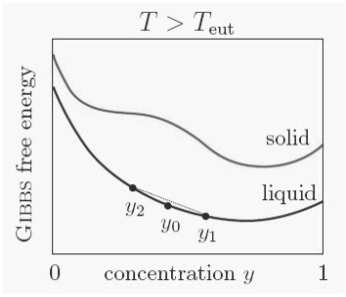

b)

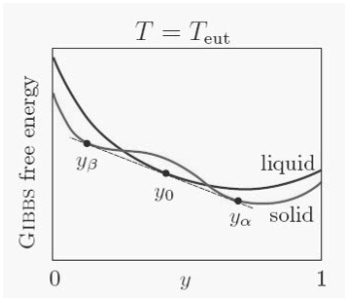

c)

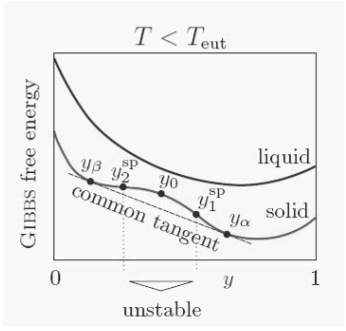

Fig. 3. Illustration of the eutectic solidification process and of the characteristic concentrations within the miscibility gap [2]

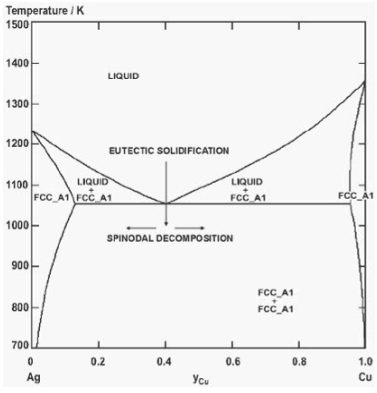

Fig. 4. Phase diagram of Ag-Cu

After the whole system reaches the equilibrium concentrations coarsening begins in such a way that the number of precipitated phase regions decreases whereas the size of the phases increases. Here the bigger phases grow at the expense of the smaller ones due to the Gibbs-Thomson effect. In particular, the concentration on the boundary of the smaller phases is greater due to the larger curvature. Consequently there is an (uphill) diffusion flux from the smaller phases to the bigger ones. This process is often called coarsening or Ostwald-ripening, and minimizes the total interfacial energy of the system [22-25].

Taking into account the above theoretical description, the purpose of this work is to study the effect of long term natural ageing processes occurring in the Ag-Cu alloy, especially on their structure and hardness linked to the spinodal decomposition occurred. Special attention was devoted to monitoring of the microstructure changes in the nanoscale of several tenth of nanometers, where the spinodal decomposition is present. In this case any artificial thermal or mechanical treatment was performed, for the reason to investigate the possibilities of mechanical properties improvement – qualified for practical use evaluation – on the basis of "natural" processes occurred in the Ag-Cu alloy.

2. Experimental procedure

The material used for investigation was a silver-copper alloy, with the chemical composition presented in Table 1. It was take from a silver coin "200 zl (XXX lat PRL) 1974r." produced in the State Mint of Poland (Mennica Państwowa) in year 1974, what gives a period of 37 year natural ageing process. The solution heat treatment effect was probably generating during hot rolling of the alloy.

Table 1.
Chemical composition of the investigated silver alloy

Chemical composition, wt. %		
Silver alloy	Ag	Cu
	62.5	37.5

The micrographs of the micro- and macrostructure investigation was performed using the light microscope Leica MEF4A supplied by Zeiss in a magnification range of 50-500x. The micrographs of the microstructures were made by means of the KS 300 program using the digital camera equipped with a special image software.

Microstructure investigation and phase identification was performed using transmission electron microscopy (TEM) JEOL JEM 3010 TEM with the bright and dark field image technique and SAD method. The diffraction pattern calculation was performed using the "Eldyf" software supplied by the Institute of Material Science of the University of Silesia.

For microstructure investigation scanning electron microscope (SEM) Zeiss Supra 25 equipped with energy dispersive spectroscope (EDS) was used. Accelerating voltage in the range of 3 to 20 kV was set, depending on the applied magnification as well the phase contrast of the areas of interest. Both the InLeans SE detector low scale magnification as well the BSD standard detector for high scale magnification were used for microstructure investigations. A working distance of ca 2 tp 10 mm was chosen for highest possible contrast achievement.

Phase, chemical composition and crystallographic structure were determined by the electron diffraction, EBSD and EDS microanalysis. EBSD parameters are chosen as following: the working distance was set to 17 mm. Number of points measure was 26800 within a field of 16.20 µm x 31.96 µm in dimension. The measurement step was set as 0.15 µm. Average Confidence Index I equal 0.00 and the Average Image Quality is equal 2454.56.

The hardness was measured with Rockwell hardness tester with a load chosen for the HRF scale, according to the PN-EN ISO 6507-1 standard, by a load of 60 Kgf with a 1/10" indenter. A minimum of 10 indentations was made on each of the tested samples.

3. Results and discussion

For phase identifications different methods were applied, one of the is the EBSD technique with results presented in Fig. 5, with silver phase detection performed in with "+" marked area in Fig. 18a. The similarity of the Ag and Cu phase makes it very difficult to distinguish between this phases based on Kikuchi lines, because of the same crystallographic A1 phase of the Fm-3m type for both silver and copper. For his reason other techniques were applied based on TEM and SEM investigations method.

Metallographic investigations of the light microscope microstructure observations are presented in Figures 6 to 9. In this small range of magnification there is visible the difference of the phase size and also a preferable orientation of the elongated phases can be recognised, caused by the initial coin production by forging. The profile of the stamping die is generating different pressure forces, which are responsible for this different areas of equal oriented phase directions and different size of the Ag_{α} and Cu_{β} phases.

Investigations results performed on transmission electron microscope, Figs. 10-17 presents the microstructure details both of the silver as well as of the copper phase. Also two strengthening mechanisms, which occur in this alloy, were confirmed. In Fig. 10 and 13 there can be recognised that slicing process occurs in the copper phase inside the grains, whereas in the silver area elongated laths can be found – Figs. 12 and 15 – with different dislocation density inside the laths. Places with high dislocation density are visible as black areas, where as uniform light grey areas are free of dislocations The visible laths have an average width of 0.1 to 0.3 µm. The observed structure presents this considerable density of dislocations affects favourably the mechanism of strengthening of the silver area. Diffraction pattern measurement (Figs. 11, 14, 16 and 17) performed for Ag and Cu phase identification give as a result the cubic phase with the group symbol 225 (Fm-3m) with zone axis [2-11] and d-spacing of 0,408 nm for silver (Fig. 17). and a cubic phase of the type 225 (Fm-3m) with zone axis [001] and d-spacing of 0.365 nm for Copper (Fig. 14).

To distinguish separately the Ag and Cu phase on a micrograph the energy dispersive microanalysis (EDS) based investigations method was applied. The results achieved in point-

wise mode are presented in Fig. 18. Using this technique it is possible to recognise both phases on a micrograph and achieved in this way the distribution of the Ag as well as the Cu phase in a macro scale. The copper phase occurs as a dark grey area in the microstructure – Figs. 18 and 18b, while the silver phase is visible on the SEM image as the white area – Figs. 18, which was confirmed by the EDS analysis in Fig. 18c.

EBSD investigations result in form of EBSD mapping presented in Fig. 19 give the overview of the grain and subgrain orientation size and placement of a relatively large area of 15 x 40 µm. In Fig. 19a there is present a mapping area in a colour scale for different orientation of the grains and subgrains. There is not any distinguished orientation of the grains present. Also any prevailing orientation can be found, but it can be seen that smaller grains are mainly connected to an other orientation compared to larger ones – where smaller grains are of the size below 5 µm.

In Figure 19b there is presented the microstructure of the investigated area with visible grey scale contrast difference inside the grains. Using back scattered electron detector it can de discovered that the grain structure itself is not uniform but consists of brighter and darker areas which can be connected to differences concerning the z-contrast, and that for some small differences in copper in silver concentration or silver in copper content.

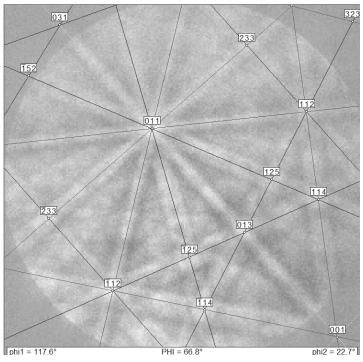

Fig. 5. EBSD detected silver phase pattern

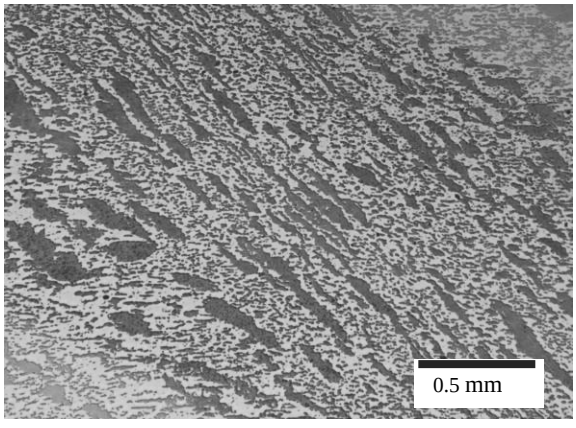

Fig. 6. Microstructure of the investigated AgCu alloy

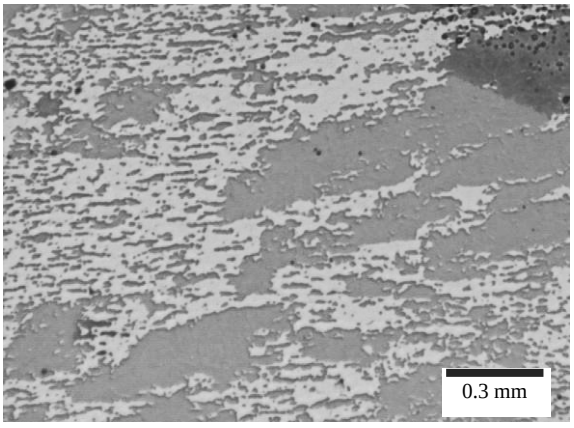

Fig. 7. Microstructure of the investigated AgCu alloy

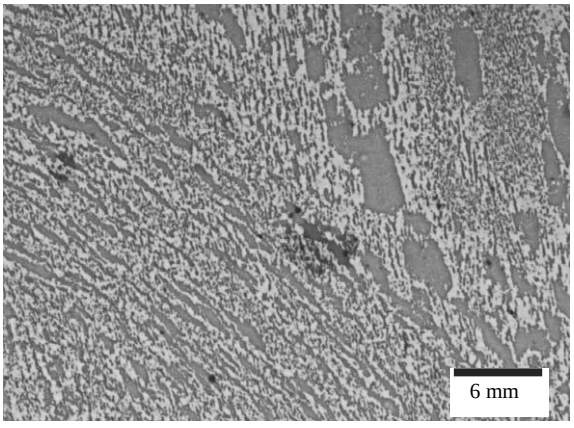

Fig. 8. Microstructure of the investigated AgCu alloy with visible plastic deformation directions

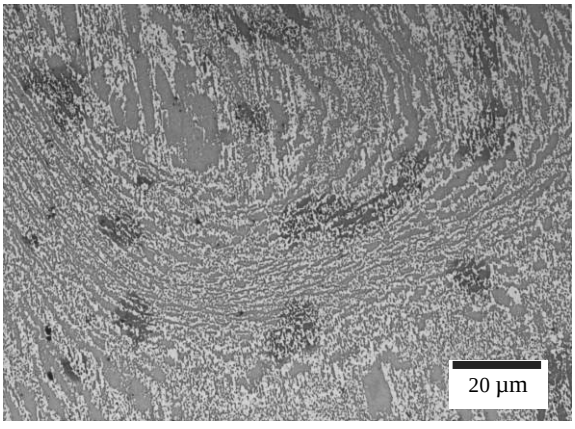

Fig. 9. Microstructure of the investigated AgCu alloy with visible plastic deformation directions

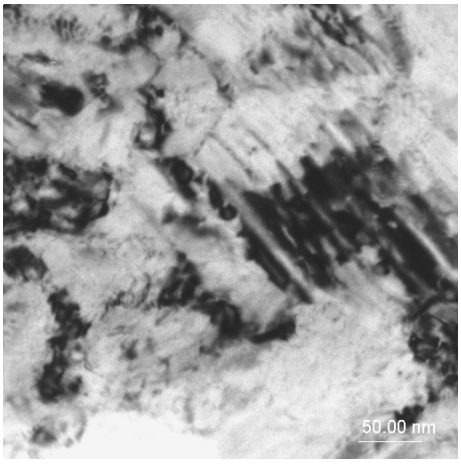

Fig. 10. Cu phase microstructure, bright field, TEM

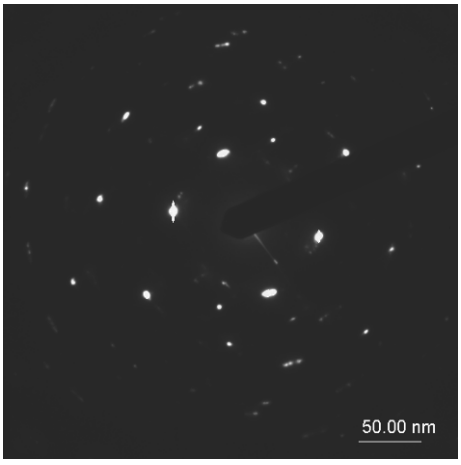

Fig. 11. Diffraction pattern of the Cu phase in [001] direction

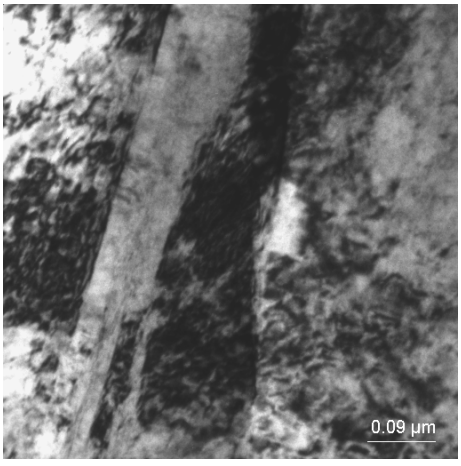

Fig. 12. Ag phase microstructure, bright field, TEM

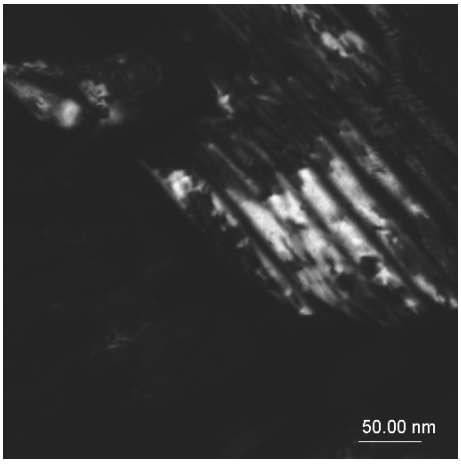

Fig. 13. Cu phase microstructure, dark field, TEM

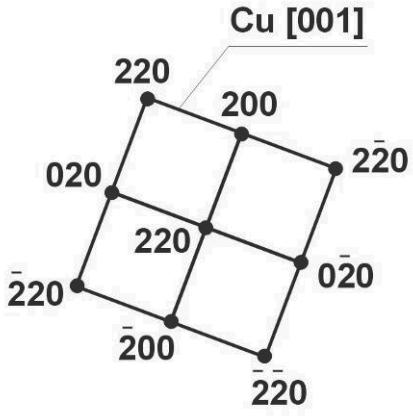

Fig. 14. Diffraction solution of pattern from Fig. 11

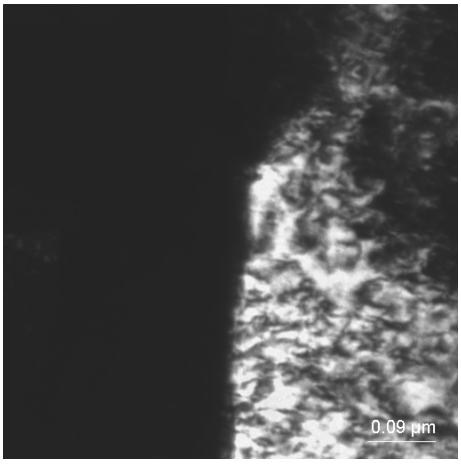

Fig. 15. Ag phase microstructure, dark field, TEM

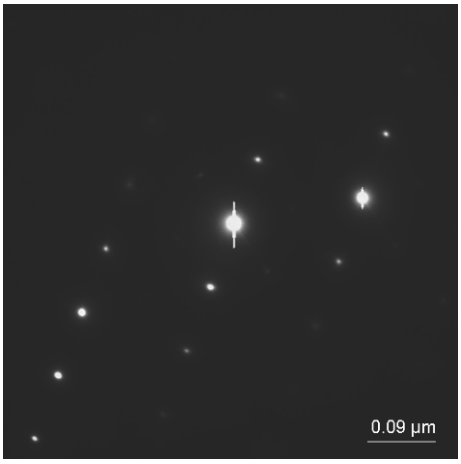

Fig. 16. Diffraction pattern of the Ag phase in [2-11] direction

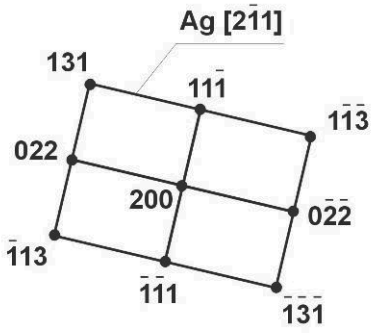

Fig. 17. Diffraction solution of pattern from Fig. 16

Figure 19c shows the blue marked grain boundaries, which are recognised using >15˚ orientation angle value. Green and red are marked subgrains boundaries with in a range of 3˚>15˚. The measurement sensitivity is set as 0.3˚, so a relatively sharp grey scale change inside of one grain, where any subgrain boundary wasn't detected, can be a boundary of a Ag lath showed in TEM micrographs with a boundary angle in the range of 0˚<0.6˚.

SEM micrographs presented in Figs. 21-26 shows the microstructure of the investigated material. In Figs. 21 and 22 there are presented the low-mag micrographs showing the shape of the shape of the Ag and Cu zones, where as in Fig. 26 there is presented the SE image of the surface, showed Silver as the white area and copper as the dark area, with very high size difference of particular Cu zones. The distribution of Ag precipitation n the Cu region seems to be of twice difference placement order (Fig. 23). On the one hand there are random place particle, on the other hand the particle are ordered in rows of ca. 20 nm distance between each other. The distance between the precipitations in a row is ca. 10 nm, and therefore smaller than the theoretically calculated spinodal decomposition distance of 15 nm, for this FCC Ag lattice In the random distributed area the average distance between the Ag precipitations is in the range between 10-40 nm (Fig. 25). In Figs. 23 and 24 there are presented areas inside the Ag matrix where Cu precipitation in only random order are placed, they are three times as big as the Cu ones, and in a distance of 30-100 nm between them, what is more the calculated 15 nm value. There is a discrepancy found both in the Cu as well Ag case, throwing new light on the spinodal decomposition behaviour difference for he same FCC lattice but for different chemical element.

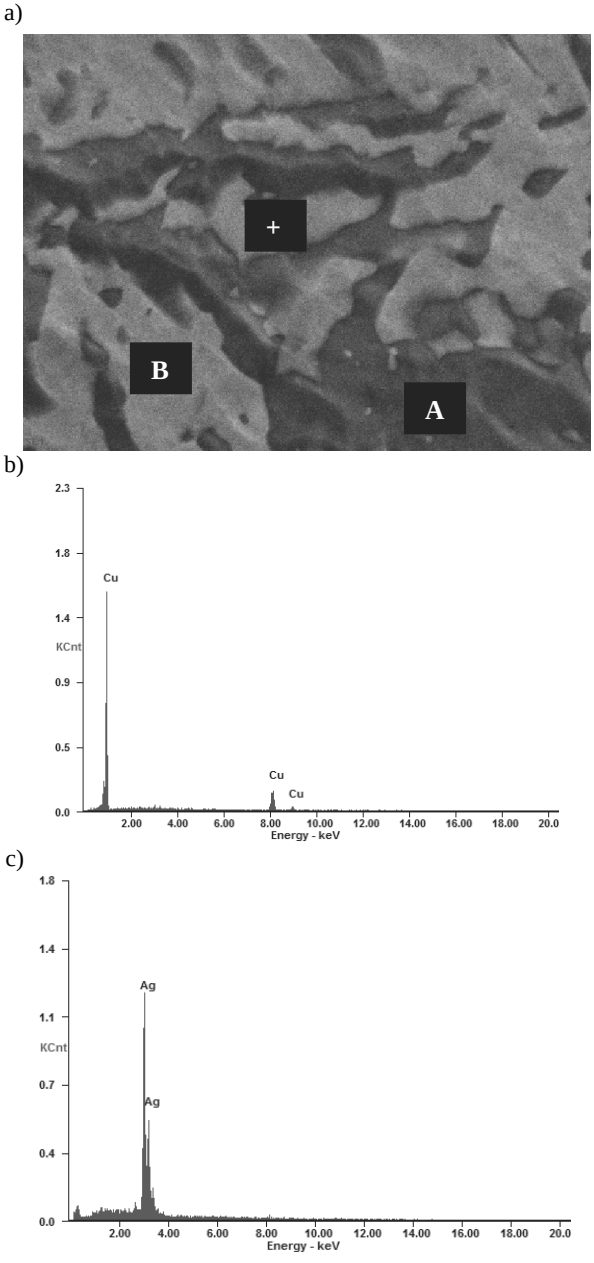

Fig. 18. EDS point-wise analysis: a) microstructure with marked places for the analysis, b) EDS microanalysis for the copper phase, (marked as A) c) EDS microanalysis for the silver phase, (marked as B)

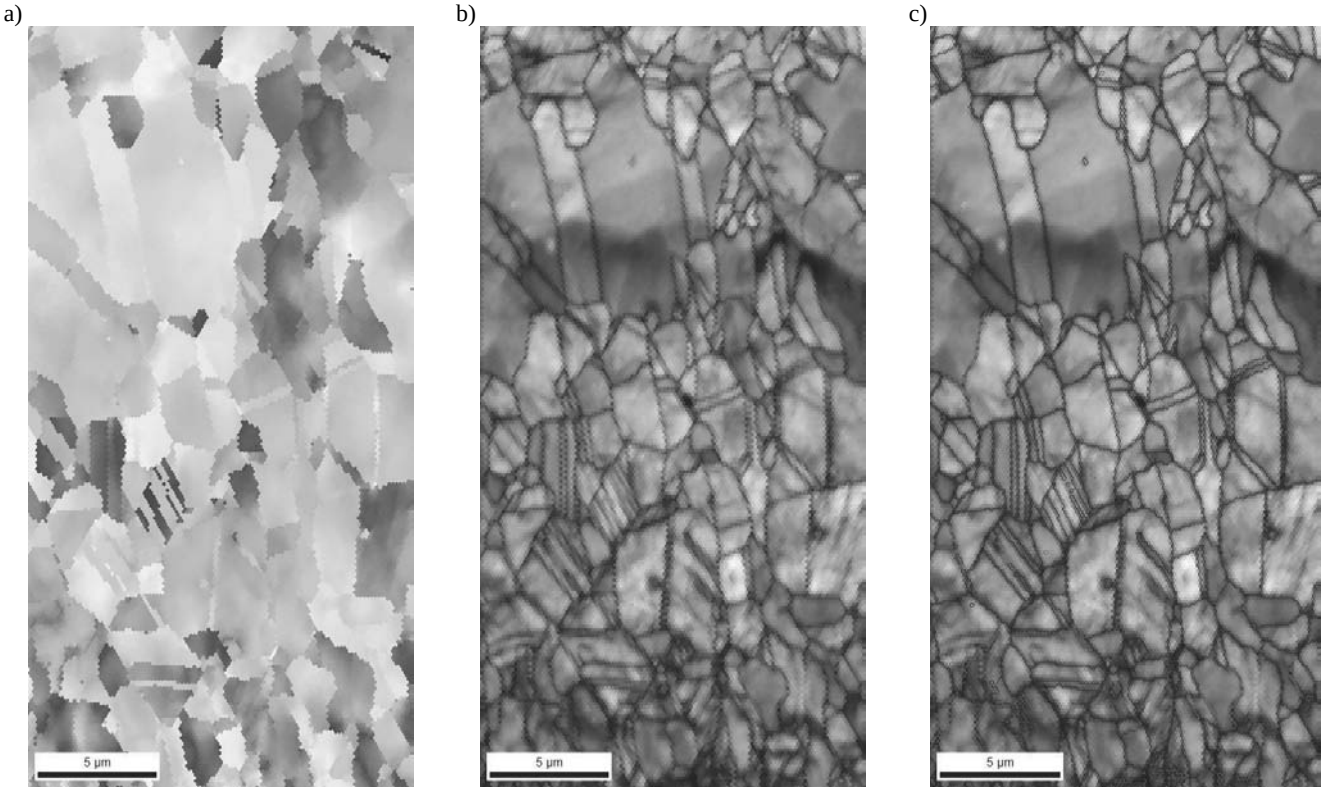

Fig. 19. EBSD mapping

The measurements were performed applying the F scale. 10 measurements were done with following values: 91,2; 80,9; 90,6; 89,3; 92,6; 90,7; 94,7; 91,7; 90,9; 85. What gives an average value of 90 HRF.

Important parameters for proper EBSD based microstructure analysis there are given the Average Fit [degrees] of 0.92, the Minimum boundary misorientation of 3.0 degrees, the Number of boundary segments of 11353, as well as the Length of boundary segments of 983.198 µm. Measured grain- and subgrain boundary length is presented in Fig. 20. Where can be recognized that in a low magnification range almost only grain boundaries are detected of a total length of 832 µm, where as subrains are measured in a total length of ca. 150 µm.

SEM microstructures give the overview and measurement possibility of the precipitations behaviour of the Ag and Cu phase. The size of the precipitations is detected as following: the Ag phase inside the Cu matrix has a globular shape with an average diameter of 30 nm, it builds parallel rows of precipitations in a distance of ca. 50 nm between the rows and ca 40 nm between the precipitations inside of a row. This placement order was found only in case of the Ag precipitations inside the Cu phase, not in a whole grain or subgrain area but partially located inside one grain. The Cu precipitations are of a size of ca. 100 nm, and there is not any placement order present, also the size range seems to be higher in a range of ca. 50 to 150 nm.

Boundaries: Rotation Angle

	Min	Max	Fraction	Number	Length
——	3°	5°	0.072	815	70.58 microns
——	5°	15°	0.081	921	79.76 microns
——	15°	180°	0.847	9617	832.86 microns

*For statistics - any point pair with misorientation exceeding 3° is considered a boundary
total number = 11353, total length = 983.20 microns)

Fig. 20. The parameters chosen for EBSD investigation

4. Conclusions

The performed investigations of the microstructure evaluation of the Ag-Cu alloy, carried out using SEM, TEM as well as light optical microscopy throw new light on the influence of long term natural ageing process on the silver-copper matrix with Ag and Cu precipitations inside the Ag_{α} and Cu_{β} matrix phase. One of the most important factors beside the initial mechanical deformation in form of forging was the decompositional process leading to a ordered placement of the Ag and Cu precipitations, having also influence on strengthening of this alloy. Particularly it can be state that:

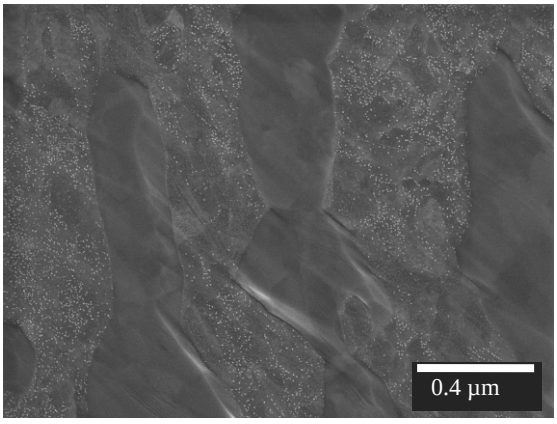

Fig. 21. Microstructure of the investigated Ag-Cu alloy with visible subgrains of the Ag and Cu phase

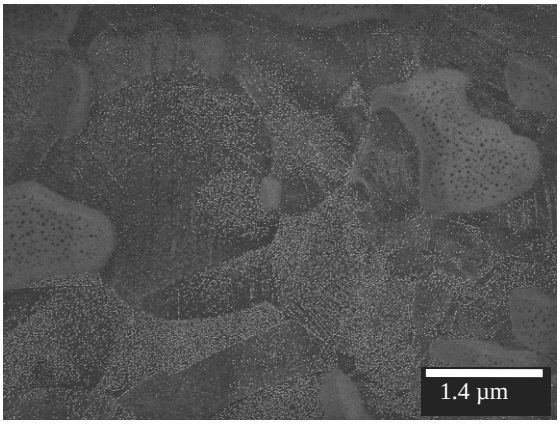

Fig. 22. Ag and Cu precipitations inside Ag and Cu matrix phase

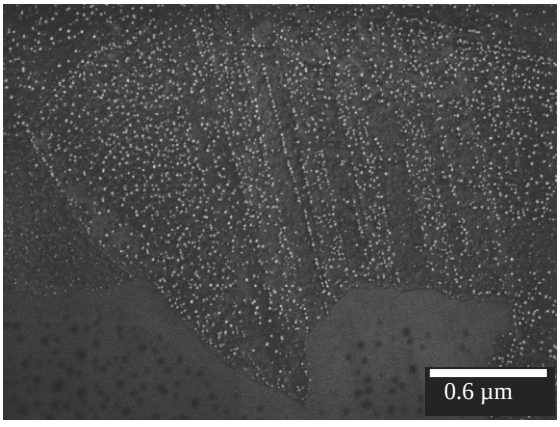

Fig. 23. Placement order of the Cu precipitations inside the Ag matrix phase

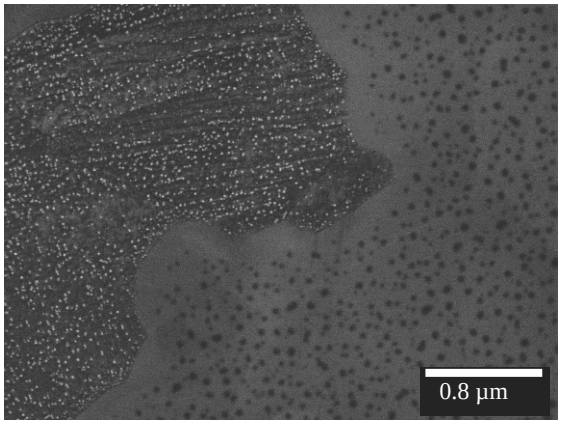

Fig. 24. Ag and Cu precipitations inside Ag and Cu matrix phase

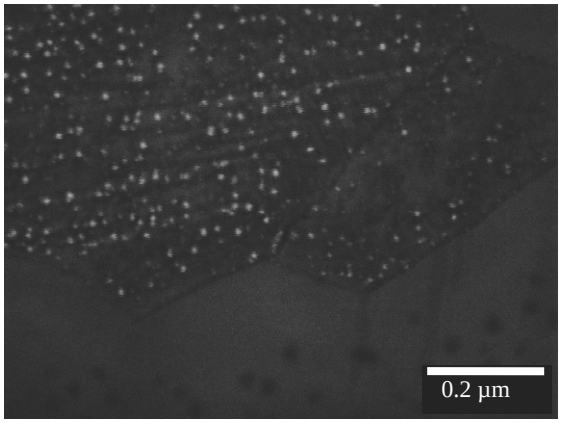

Fig. 25. Size difference of the Cu precipitations inside the Ag matrix phase

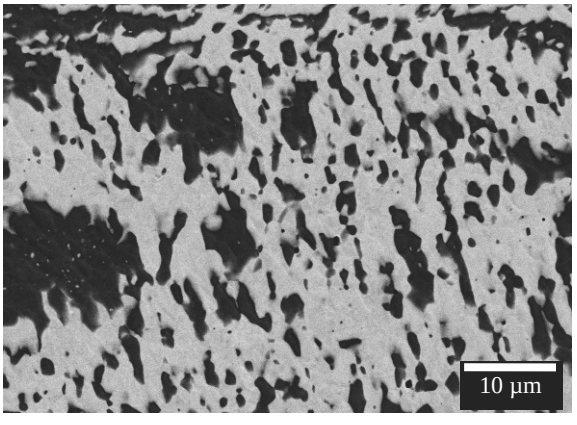

Fig. 26. Low magnification microstructure of the investigated Ag-Cu alloy

(1) the investigated Ag-Cu alloy is characterised with a structure of Ag and Cu grains with subgrain structure, recognised as dark Cu areas and white Ag areas detected using the EDS technique in the SEM microscope,
(2) the investigated alloy has average hardness value of 90 HRF after long term ageing in room temperature,
(3) the precipitated globular shaped nanocrystalline Cu phase inside the Ag matrix has a average size of ca. 15 nm in diameter, whereas the detected globular shaped nanocrystalline Ag phase inside the Cu matrix has a average size of ca. 45 nm in diameter,
(4) within the Cu phase there are found some twinned areas confirmed using diffraction pattern calculations, bright and dark field TEM techniques,
(5) within the Ag phase there are found place with very high dislocations density by mind of TEM thin foils investigations.

Acknowledgements

The author will express his great thanks to Dr Eng. Krystian Prusik PhD, assistant professor in the Division of Structure Studies, Institute of Materials Science, Faculty of Computer and Materials Science, University of Silesia, Katowice for scientific support in elaboration of this work.

References

[1] P. Galenko, D. Danilov, V. Lebedev, Phase-field-crystal and Swift-Hohenberg equations with fast dynamics, Physical Review E 79 (2009) 52-56.
[2] T. Boehme, Investigations of Microstructural Changes in Lead-Free Solder Alloys by Means of Phase Field Theories, doctoral thesis, Berlin, 2008.
[3] www.personal.psu.edu
[4] H.X. Li, X.J. Hao, G. Zhao, S.M. Hao, Characteristics of the continuous coarsening and discontinuous coarsening of spinodally decomposed Cu-Ni-Fe alloy, Journal of Materials Science 36 (2001) 779-784.
[5] C.E. Cordeiro, J.B. Silva, S. Moss de Oliveira, A. Delfino, J.S. Sá Martins, Nucleation Processes Close to the Spinodal, International Journal of Thermophysics 28/4 (2007) 1269-1274.
[6] M. Hättestrand, P. Larsson, G. Chai, J. O. Nilsson, J. Odqvist, Study of decomposition of ferrite in a duplex stainless steel cold worked and aged at 450-500 °C, Materials Science and Engineering A 499 (2009) 489-492.
[7] J. Stobrawa, Z. Rdzawski, W. Głuchowski, Microstructure and properties of nanocrystalline copper–yttria micro-composites, Journal of Achievements in Materials and Manufacturing Engineering 24/2 (2007) 83-86.
[8] J. Stobrawa, Z. Rdzawski, Dispersion – strengthened nanocrystalline copper, Journal of Achievements in Materials and Manufacturing Engineering 24/2 (2007) 35-42.
[9] X.Y. Sun, L. Zhen, C.Y. Xu, L.X. Lv, W.Z. Shao, X.D. Sun Mössbauer spectrometry study of early stage spinodal decomposition in Fe–Cr–Co alloy under high magnetic field, Materials Letters 63 (2009) 64-65.
[10] K. Labisz, M. Krupiński, L.A. Dobrzański, Phases morphology and distribution of the Al-Si-Cu alloy, Journal of Achievements in Materials and Manufacturing Engineering 37/2 (2009) 309-316.
[11] L.A. Dobrzański, M. Krupiński, K. Labisz, Derivative thermo analysis of the near eutectic Al-Si-Cu alloy, Archives of Foundry Engineering 8 (2008) 37-40.
[12] L.A. Dobrzański, M. Krupiński, K. Labisz, B. Krupińska, A Grajcar, Phases and structure characteristics of the near eutectic Al-Si-Cu alloy using derivative thermo analysis, Materials Science Forum 638-642 (2010) 475-480.
[13] L.A. Dobrzański, K. Labisz, R. Maniara, A. Olsen, Microstructure and mechanical properties of the Al-Ti alloy with cerium addition, Journal of Achievements in Materials and Manufacturing Engineering 37/2 (2009) 622-629.
[14] K.H. Lo, J.K.L. Lai, Microstructural characterisation and change in a.c. magnetic susceptibility of duplex stainless steel during spinodal decomposition, Journal of Nuclear Materials 401 (2010) 143-148.
[15] T. Tański, L.A. Dobrzański, K. Labisz, Investigation of microstructure and dislocations of cast magnesium alloys, Journal of Achievements in Materials and Manufacturing Engineering 42 (2010) 94-102.
[16] B. Krupińska, K. Labisz, L.A. Dobrzański, Z. Rdzawski, Microstructure investigation cast zinc alloys modified with Ce, La, St, Ti, B, Journal of Achievements in Materials and Manufacturing Engineering 42 (2010) 50-57.
[17] J. Wang, H. Zou, C. Li, S. Qiub, B. Shen, The spinodal decomposition in 17-4PH stainless steel subjected to long-term aging at 50 °C, Materials Characterization 59 (2008) 587-591.
[18] Z. R. Liu, H. Gao, A differential cluster variation method for analysis of spinodal decomposition in alloys, The European Physical Journal B 37/3 (2004) 369-374.
[19] K. Shen, Z.M. Yin, T. Wang, On spinodal decomposition in ageing 7055 aluminum alloys, Materials Science and Engineering A 477 (2008) 395-398.
[20] J.C. Zhao, M.R. Notis, Ordering Transformation and Spinodal Decomposition in Au-Ni Alloys, Metallurgical And Materials Transactions 30 (1999) 707-716.
[21] S. Rusz, K. Malanik, Refining of structure of the alloy AlMn1Cu with use of multiple severe plastic deformation, Journal of Achievements in Materials and Manufacturing Engineering 27/2 (2008) 167-178.
[22] M.B. Kannan, Influence of microstructure on the in-vitro degradation behaviour of magnesium alloys, Materials Letters 64 (2010) 739-742.
[23] T. Tański, L.A. Dobrzański, R. Maniara, Microstructures of Mg-Al-Zn and Al–Si–Cu cast alloys, Journal of Achievements in Materials and Manufacturing Engineering 38/1 (2010) 64-71.
[24] M. Goral, G. Moskal, L. Swadzba, Gas phase aluminising of TiAl intermetallics, Journal of Achievements in Materials and Manufacturing Engineering 20 (2007) 443-446.
[25] D. Ovono Ovono, I. Guillot, D. Massinon, The microstructure and precipitation kinetics of a cast aluminium alloy, Scripta Materialia 55 (2006) 259-262.